The Two-Dimensional Pore and Polarization Transport Model to Describe Mixtures Separation by Nanofiltration: Model Validation

S. Déon
Institut UTINAM (UMR CNRS 6213), Université de Franche-Comté, Besançon cedex 25030, France

P. Dutournié and L. Limousy
Laboratoire d'Ingénierie des MATétiaux de Bretagne (LIMAT^{B}—EA 4250), Université de Bretagne Sud, rue de Saint-Maudé, BP 92116, Lorient 56 321, France

P. Bourseau
Laboratoire d'Ingénierie des MATétiaux de Bretagne (LIMAT^{B}—EA 4250), Université de Bretagne Sud, rue de Saint-Maudé, BP 92116, Lorient 56 321, France
Laboratoire de Génie des Procédés Environnement-Agroalimentaire (GEPEA—UMR CNRS 6144), Université de Nantes, BP 406, Saint-Nazaire 44602, France

DOI 10.1002/aic.12330
Published online July 20, 2010 in Wiley Online Library (wileyonlinelibrary.com).

Nanofiltration is a membrane process which is used to separate charged molecules such as ions. Even if this process is well known, there is no mean to predict the performances of a given separation. The aim of this paper is to present a two-dimensional model called "pore and polarization transport model" which includes all the steps of the ions transfer. The membrane transport modeling is based on the classical one-dimensional vision coupling the Donnan, steric, and dielectric exclusions with the extended Nernst-Planck transport equation. But the originality of this study comes from the modeling of the transport through the polarization layer. The model used in this study is an improvement of the previous version, which includes an electrical gradient within the polarization layer allowing the prediction of polarization layer establishment even for ionic mixtures. The purpose of this article is to describe the model accurately before validating it with various ionic solutions. © 2010 American Institute of Chemical Engineers *AIChE J,* 57: 985–995, 2011
Keywords: nanofiltration, transport phenomena, polarization layer, turbulent flow, 2-D model, Nernst-Planck equation, ionic mixtures

Introduction

Nanofiltration (NF) is a membrane separation process which finds many applications in industrial and environmental purposes. It has intermediate properties between those of reverse osmosis and ultrafiltration. For this reason, NF is perfectly suitable to fractionate small molecules according to their size as well as their electrical charge. NF membranes are thus widely used in various fields, particularly in the production of drinking water to remove undesirable compounds such as pesticides or monovalent anions (Van der Bruggen et al.[1,2]), with probably a special attention paid to defluoridation to solve problems related to high fluoride concentrations in drinking water in rural areas of many countries (Pontié et al.[3]). NF can also be an interesting solution to selectively demineralize salted water to produce isotonic waters (Oumar

Correspondence concerning this article should be addressed to S. Déon at sebastien.deon@univ-fcomte.fr.

Anne et al.,[4] Pontié et al.[5]) and for the treatment of food ingredients solutions such as seafood aromas concentration (Walha et al.[6]) or peptides solutions concentration (Bourseau et al.[7]). Prediction of separation performances is an important way of improvement and a predictive model could be a very useful tool for process development and optimization, or for membranes characterization with the aim to provide help to end-users for the selection of commercial membranes for water desalination (Pontié et al.[8]). Many authors have studied the mass transfer through membranes in the last few years. It is usually admitted that the transfer through the membrane can be described by such models, but their use is very limited because many assumptions and boundary conditions exist. One of these boundary conditions is the concentration polarization layer and transport in this layer is less frequently investigated. Indeed, polarization is often neglected (Hagmeyer and Gimbel,[9] Tanninen et al.[10]), estimated from empirical formulations (Gekas and Olund,[11] Afonso and De Pinho[12]), or assessed by an indirect method from experimental data, e.g., by studying the rejection evolution with velocity variation method (VVM; Morão et al.,[13] Jonsson and Boesen[14]). Some authors have developed knowledge models to describe the layer establishment and two ways are usually adopted. The former consists in considering the polarization layer as a membrane with infinite porosity and modeling the fluxes by the extended Nernst-Planck equation (Geraldes and Afonso,[15] Morão et al.[16]). This approach shows two main disadvantages. First, solving equations requires the estimation of the layer thickness, which appears to be complicated for ionic mixtures (i.e., one thickness per ion). Second, the transport is modeled monodimensionally, and the heterogeneity along the membrane is thus not described (i.e., axial convective transport is fully neglected). The second approach available in literature is based on a two-dimensional (2-D) study state mass balance in the flow, but this way is appropriate only for pure salt mixtures by considering a mean salt diffusivity (Bhattacharjee et al.,[17] Pak et al.[18]). The pore and polarization transport model (PPTM) presented in this article is a combination of these two approaches. Transport is modeled with a 2-D differential steady-state mass balance but including an electromigrative term to balance the difference between ion diffusivities and to respect electroneutrality within the solution. For better description of the polarization establishment, this model also includes the variation of activity coefficients in the polarization layer.

This model could thus be very useful to predict experimental rejection of ionic mixtures as polarization phenomenon occurs even when one tries to minimize it. The PPTM could thus be used for industrial applications concurrently to the introduction of factors used by some authors (Verliefde et al.[19]). Moreover, with this model, membrane length can be taken into account, and polarization phenomenon could be investigated without necessity of many experiments.

In this article, the model development is first precisely described before been validated by comparing experimental real and observed rejection with model predictions in the case of pure salt solutions, ternary and quaternary mixtures.

Modeling development

The model proposed in this article is based on the first version of the PPTM previously presented (Déon et al.[20]). The predictive model presented in this article is a 2-D modeling of transport through the polarization layer including a one-dimensional (1-D) modeling of transport within the membrane pores as subroutine.

The 1-D modeling of transport within the pores presented in this article is based on the Donnan steric pore model proposed by Bowen et al.[21,22] for which the solute transport is described as resulting of the transport through the membrane and equilibrium partitioning at the membrane interface. Separation selectivity also depends on solute accumulation close to the membrane wall, called polarization phenomenon, which is described by the 2-D model. The first version of this phenomenological model which was called PPTM is suitable only for the filtration of pure salt solutions. In this article, a new version of the PPTM including an electromigration transfer in the polarization layer induced by the differences of various ions diffusivities is developed. The solute accumulation at the membrane wall involves the definition of two rejections, i.e., the real rejection $R_{i,\mathrm{m}}$ and the observed rejection $R_{i,\mathrm{obs}}$. The former is an experimental value depending on hydrodynamic conditions in the retentate flow, and the latter is an intrinsic data of the membrane-solution couple.

$$R_{i,\mathrm{obs}} = 1 - \frac{C_{i,\mathrm{p}}}{C_{i,\mathrm{r}}} \tag{1}$$

$$R_{i,\mathrm{m}} = 1 - \frac{C_{i,\mathrm{p}}}{C_{i,\mathrm{w}}} \tag{2}$$

where $C_{i,\mathrm{p}}$ and $C_{i,\mathrm{r}}$ are respectively the concentrations in permeate and retentate streams, and $C_{i,\mathrm{w}}$ is the concentration at the membrane wall.

The PPTM is also able to describe the volumetric permeation flux J_v through Eq. 3 and both real and observed rejections for given feed concentrations $C_{i,\mathrm{r}}$, applied pressure ΔP and tangential velocity U_t.

$$J_\mathrm{v} = \frac{L_\mathrm{p}}{\eta}(\Delta P - \Delta\pi) \tag{3}$$

L_p, η and $\Delta\pi$ are respectively the membrane permeability, the viscosity, and the osmotic pressure difference deduced from Van't Hoff relation (Eq. 4).

The various steps of the transfer and the corresponding equations are presented below. The numerical procedure for solving the PPTM is sum up on Figure 1 and equations not written in the text are given in Table 1.

1-D membrane transport

The distribution of ions at the membrane inlet and outlet is described in the model by an equilibrium partitioning established between the solutions on both sides of the membrane-solution interfaces. This equilibrium between concentrations in the bulk solution C_{ii} and the concentrations in the pores c_i results from electrochemical potential equality,[23] molecular interaction by means of activity coefficients γ_i, and finally steric and dielectric effects.

$$\frac{c_i}{C_i} = \frac{\gamma_{i,\mathrm{s}}}{\gamma_{i,\mathrm{m}}}\phi_i \exp(-\Delta W_i)\exp\left(\frac{-z_i F}{\mathrm{RT}}\Delta\psi_\mathrm{D}\right) = \phi_i' \exp\left(\frac{-z_i F}{\mathrm{RT}}\Delta\psi_\mathrm{D}\right) \tag{5}$$

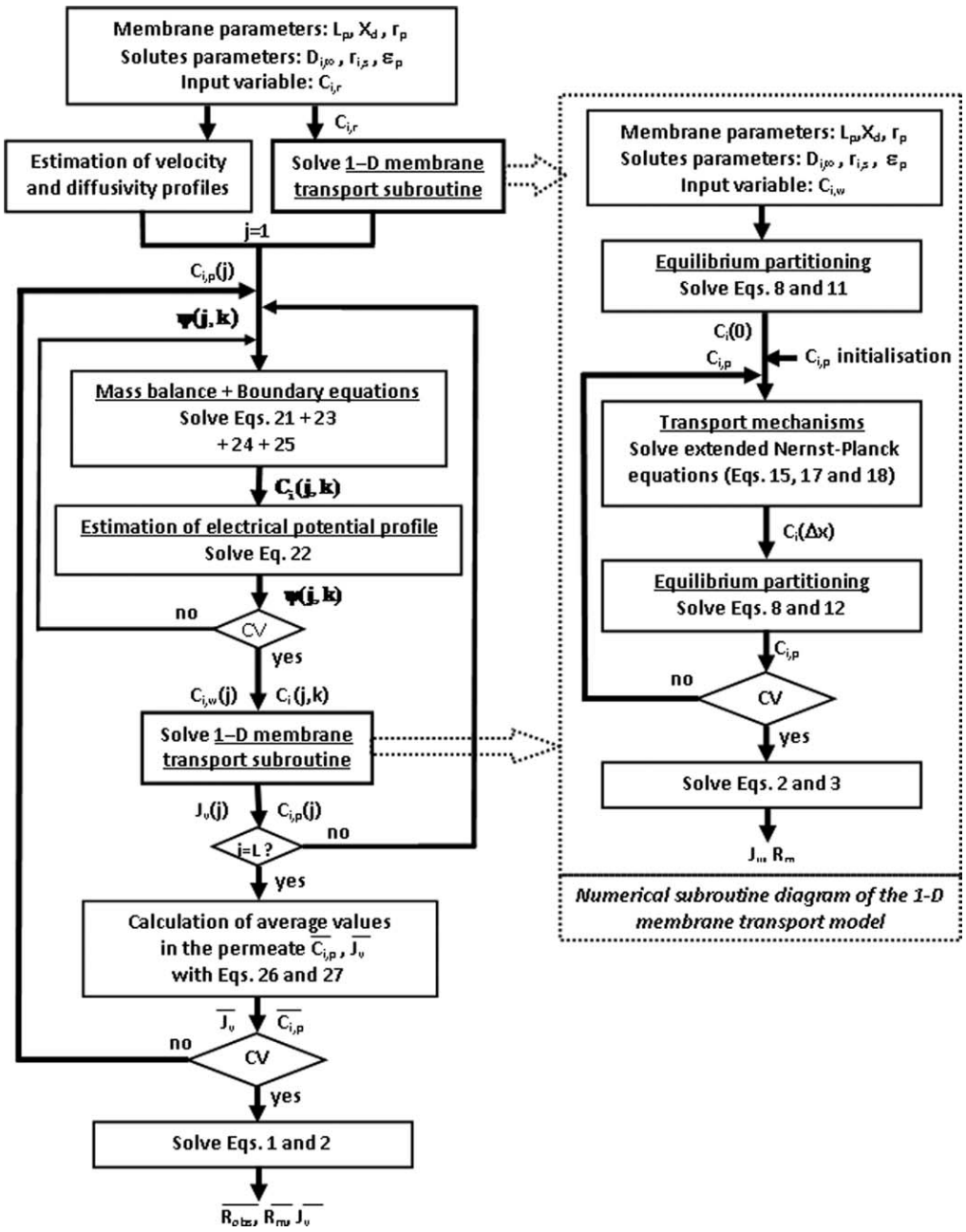

Figure 1. Numerical procedure diagram of 2-D PPTM combining polarization and membrane transports.

where ϕ_i is the steric partitioning coefficient defined by Ferry[24] which depend on the ratio between the radius of solutes and that of pores (Eq. 6). In this model, a single mean pore size is considered but model could probably be improved by introducing a pore size distribution as those found by Van der Bruggen and Vandecasteel[25] or Aimar et al.[26] ΔW_i represents the solvation energy barrier generated by all the physicochemical interactions between ions and membrane material and between ions themselves. This term thus includes both confinement, the so-called ''image forces,'' influence of membrane charge and physico-chemical environment. This article is mainly focused on the polarization layer, and so, this solvation energy increase within the pores is modeled by a decrease of the effective dielectric constant of the solution ε_p. So within the scope of the PPTM, the solvation energy barrier in the partitioning is described by the Born model[27] (Eq. 7) describing the influence of the difference between the dielectric constants of the free solution ε_s and that of the solution within the pores ε_p. It should be specified that interactions between ions and the ''image charges'' generated at interfaces having different dielectric properties[28,29] can be studied a posteriori by dissociating the various contributions acting on the solvation energy.

The so-called Donnan potential $\Delta\psi_D$ is the electrical gradient between both sides of the interface, and its value is the same whatever the ion considered. So, Eq. 5 written for two ions in solution (i and j) leads to the equilibrium partitioning between these two ions:

Table 1. Equations Used in the 1-D Model of Membrane Transport

Van't Hoff Equation	$\Delta\pi = \mathrm{RT}\sum_{i=1}^{n}(C_{i,w} - C_{i,p})$ (4)
Steric partitioning	$\phi_i = \left(1 - \frac{r_i}{r_p}\right)^2$ (6)
Born solvation energy barrier	$\Delta W_i = \frac{z_i^2 e^2}{8\pi\varepsilon_0 k_B T r_i}\left(\frac{1}{\varepsilon_p} - \frac{1}{\varepsilon_b}\right)$ (7)
Equilibrium partitioning	$\left(\frac{c_i}{\phi_i' C_i}\right)^{\frac{1}{z_i}} = \left(\frac{c_j}{\phi_j' C_j}\right)^{\frac{1}{z_j}}$ (8)
Electroneutrality in the bulk solution	$\sum_{i=1}^{n} z_i C_i = 0$ (9)
Electroneutrality within the pores	$\sum_{i=1}^{n} z_i c_i + X_d = 0$ (10)
Equilibrium partitioning at the pore inlet	$z_1 c_1(0) + \sum_{j=2}^{n}\left[z_j \phi_j' C_{j,w}\left(\frac{c_1(0)}{\phi_1' C_{1,w}}\right)^{z_i/z_1}\right] + X_d = 0$ (11)
Equilibrium partitioning at the pore outlet	$z_1 C_{1,p} + \sum_{1}^{n}\left[\frac{z_i c_i(\Delta x)}{\phi_i'}\left(\frac{c_1(\Delta x)}{\phi_1' C_{1,p}}\right)^{-z_i/z_1}\right] = 0$ (12)
Hindered coefficient for diffusion	$K_{i,d} = 1 - 2,30\lambda_i + 1,154\lambda_i^2 + 0,224\lambda_i^3$ (13a)
Hindered coefficient for convection	$K_{i,c} = (2-\phi)(1 + 0,054\lambda_i - 0,988\lambda_i^2 - 0,441\lambda_i^3)$ (13b)
Hagen-Poiseuille	$V = \frac{r_p^2[\Delta P - \Delta\pi]}{8\eta\Delta x}$ (15)
Mass conservation of ion i	$j_i = VC_{i,p}$ (16)
Concentration gradient calculation	$\frac{dc_i}{dx} = \frac{V}{D_{i,p}}\left(K_{i,c}c_i - C_{i,p}\right) - \frac{z_i c_i}{RT}F\frac{d\psi}{dx}$ (17)
Electrical gradient calculation	$\frac{d\psi}{dx} = \frac{\sum_{i=1}^{n}\frac{z_i V}{D_{i,p}}\left(K_{i,c}c_i - C_{i,p}\right)}{\frac{F}{RT}\sum_{i=1}^{n} z_i^2 c_i}$ (18)

$$\left(\frac{c_i}{\phi'_{iC_i}}\right)^{\frac{1}{z_i}} = \left(\frac{c_j}{\phi_{j'C_j}}\right)^{\frac{1}{z_j}} \quad (8)$$

The concentrations at the pore inlet $c_i(0)$ are calculated knowing the wall concentration $C_{i,w}$ by solving Eq. 11. Concentrations of the others ions j at the pore inlet are calculated through the Eq. 8 knowing the $c_1(0)$. The same procedure is used to calculate permeate concentrations from concentrations $c_i(\Delta x)$ at the pore outlet with Eq. 12.

The transfer of ions through the membrane is described as the transport of solid spheres within cylindrical and uniformly dispersed nanometer-sized pores. The fluxes of the various ions can be defined as the result of three fluxes due to diffusion, electromigration, and convection. Ions fluxes can thus be described by the extended Nernst-Planck equation[30,31] modified to take the influence of pores wall on diffusive and convective transports into account, by introducing hindered factors for diffusion $K_{i,d}$ and convection $K_{i,c}$[32,33] calculated with Eqs. 13a and 13b. The flux of a component i (j_i) in the pore axial direction x can thus be written as[34]:

$$j_i = -K_{i,d}D_{i,\infty}\frac{dc_i}{dx} - \frac{z_i c_i K_{i,d} D_{i,\infty}}{RT}F\frac{d\psi}{dx} + K_{i,c}c_i V \quad (14)$$

with c_i and $D_{i,m}$, respectively, the concentration and the molecular diffusivity of ith ion, $\frac{d\psi}{dx}$ the electrical gradient along

the pore. V is the solvent velocity within the pore which can be estimated by the Hagen-Poiseuille equation (Eq. 15).

Equations 17 and 18 are solved to simultaneously to determine the concentration profiles along the pores. Then, permeate concentrations are calculated with equilibrium partitioning at the outlet interface and this procedure iterated until convergence on $C_{i,\mathrm{p}}$.

2-D transport in the polarization layer

The originality of this article is based on the 2-D modeling of the concentration polarization phenomenon. This polarization phenomenon is due to permeation flux through the membrane which involved solute accumulation close to the wall. This concentration increase from bulk concentrations ($C_{i,\mathrm{r}}$) to wall concentrations ($C_{i,\mathrm{w}}$) plays an important role on the separation performances which were also found to vary along the membrane length.[20] Correctly modeled the establishment of the polarization layer appears thus to be a major step to predict mixture separation. It is thus primordial to accurately describe the transport phenomena occurring in the mass layer. Usually, polarization layer is assessed by a general approach calculating the effect of concentration polarization through dimensionless numbers[35] (e.g., Peclet, Sherwood, Reynolds, Schmidt). This classical approach can give a good approximation especially when it is coupled with experimental measurements,[36] but it does not take account of layer heterogeneity along the membrane. Second, this general approach is not viable for ionic mixtures as it leads to one layer thickness per ion which is not the case in reality. For this purpose, a 2-D modeling of this layer is proposed, including the influence of turbulence on the velocity profile and the diffusivities at the membrane wall. Models proposed in the literature (Bhattacharjee et al.[37]) were developed to describe the transport of pure salt mixtures by considering a mean salt diffusivity and assuming that the ion fluxes can be modeled by the Fick's law. This vision is valid for pure salt solutions, but in the case of mixtures, ions have to be considered independently. Indeed, ions diffuse at different velocities, so that an electrical contribution has to be taken into account to respect electroneutrality in the layer. In this article, a complete model valid even for ions mixtures is presented where the flux through the polarization layer is described by the so-called extended Nernst-Planck equation. The variation of activity coefficients γ_i within the layer was also included in the model, and so the flux of an ion i can be written as:

$$\vec{J}_i = -C_i D_{i,\mathrm{eff}} \vec{\nabla}(\ln \gamma_i) - D_{i,\mathrm{eff}} \vec{\nabla} C_i - \frac{z_i C_i D_{i,\mathrm{eff}}}{\mathrm{RT}} F \vec{\nabla}\psi + C_i \vec{V} \tag{19}$$

where $\vec{V}\big|_v^u$ is the velocity vector with u and v, respectively, the radial (y) and axial (z) components. ψ is the electrical potential and $D_{i,\mathrm{eff}}$ is the effective diffusivity defined from the pseudo-laminar model as the sum of molecular and eddy diffusivities. Indeed, effect of turbulence is introduced in the buffer and inertial layers through the turbulent diffusivity $D_{i,\mathrm{t}}$ estimated from turbulent viscosity by Prandtl's mixing length.[38] Velocity profile in the various sub-layers is determined from classical hydrodynamic equations for turbulent flow in tubular pipe.[39]

The concentration profiles in the polarization layer are obtained with a steady-state differential mass balance for each ion:

$$\nabla \vec{J}_i = 0 \tag{20}$$

Introducing Eq. 19 in Eq. 20 gives for an ion i:

$$\begin{aligned}\nabla(\vec{J}_i) = 0 = &-C_i D_{i,\mathrm{eff}} \Delta(\ln \gamma_i) - D_{i,\mathrm{eff}} \vec{\nabla} C_i . \vec{\nabla}(\ln \gamma_i) - D_{i,\mathrm{eff}} \Delta C_i \\ &- \frac{z_i C_i D_{i,\mathrm{eff}}}{\mathrm{RT}} F \Delta\psi - \frac{z_i D_{i,\mathrm{eff}}}{\mathrm{RT}} F \vec{\nabla} C_i . \vec{\nabla}\psi + \vec{V} . \vec{\nabla} C_i \end{aligned} \tag{21}$$

Equation 21 is used to calculate the ions concentrations in the polarization layer and the electrical potential gradient $\vec{\nabla}\psi$ is estimated by considering $\sum_{i=1}^{n} zi \nabla \vec{J}i = 0$:

$$\begin{aligned}&- \sum_{i=1}^{n} C_i D_{i,\mathrm{eff}} z_i \Delta(\ln \gamma_i) - \sum_{i=1}^{n} D_{i,\mathrm{eff}} z_i \vec{\nabla} C_i . \vec{\nabla}(\ln \gamma_i) \\ &\quad - \sum_{i=1}^{n} D_{i,\mathrm{eff}} z_i \Delta C_i - \frac{F}{\mathrm{RT}} \sum_{i=1}^{n} D_{i,\mathrm{eff}} z_i^2 C_i \Delta\psi \\ &\quad - \frac{F}{\mathrm{RT}} \sum_{i=1}^{n} D_{i,\mathrm{eff}} z_i^2 \vec{\nabla} C_i . \vec{\nabla}\psi + \underbrace{\vec{V} . \sum_{i=1}^{n} z_i \vec{\nabla} C_i}_{=0} = 0 \end{aligned} \tag{22}$$

The electrical potential gradient is inserted in Eq. 21, and the procedure is reiterated until convergence on the concentrations and electrical potential profiles.

Permeate concentrations $C_{i,\mathrm{p}}$, estimated with the 1-D membrane subroutine, are used to define the boundary conditions at the membrane wall:

$$\vec{J}_{\mathrm{v}}\left(C_{i,\mathrm{w}} - C_{i,\mathrm{p}}\right) = -C_i D_{i,\mathrm{w}} \vec{\nabla}(\ln \gamma_i) - D_{i,\mathrm{w}} \vec{\nabla} C_i - \frac{z_i C_i D_{i,\mathrm{w}}}{\mathrm{RT}} F \vec{\nabla}\psi_i \tag{23}$$

Equation 23 is summed for all ions to estimate the electrical gradient until convergence on the wall concentrations $C_{i,\mathrm{w}}$. It should be noticed that all the concentrations are linked together by means of the electroneutrality equation (Eq. 9).

The study of pure salt solutions[40] has shown that experimental tendencies can only be predicted by adjusting the diffusivity of the salt at the wall $D_{i,\mathrm{w}}$ in the boundary equation (Eq. 23). This so-called "wall diffusivity" becomes a polarization model parameter, and its values were reassessed by fitting experimental data obtained with salt experiments and validated with others. This "wall diffusivity" was found to be independent of salt and concentration, and it was also shown that it increases linearly with tangential velocity U_{t}. This increase in diffusivity is assumed to be due to hydrodynamic phenomena such as membrane roughness or suction and is thus linked to the tangential velocity U_{t} by:

$$D_{i_{,\mathrm{w}}} = \alpha(U_{\mathrm{t}}) D_{i,\mathrm{m}} \tag{24}$$

where α is a coefficient representing the influence of velocity on diffusivity in Eq. 24.

Previous studies showed that this diffusivity increase is probably an hydrodynamic phenomenon as α-value was

found to vary linearly with the tangential velocity U_t. α-value can thus be estimated by the empirical relation (Eq. 25) which was identified and validated with the first version of the PPTM on various salts and concentrations in previous articles.[20,40]

$$\alpha = 0.55\,U_t + 1.55 \tag{25}$$

This parameter is not clearly physically explained but a sensitivity study showed that the sole way to correctly describe influence of pressure and velocity on rejection is to increase the diffusivity value in the boundary equation (Eq. 23). It seems that the influence of the membrane wall on the ions exclusion is not fully described by the model. One of the hypothesis could be an hydrodynamic phenomena as this increase seemed to vary linearly with the tangential velocity. This increase could be due to the turbulence induced by the porosity and the roughness of the membrane wall. For example, some authors have observed a diffusivity increase of particles induced by the shear (Eickstein et al.[41]) and others have found that the transfer coefficient can increase with the roughness of a biofilm (Picioreanu et al.[42]).

Boundary conditions outside of the layer ($y > \delta$) are defined by:

$$z = 0, \forall y \qquad C_i(0,y) = C_{i,r} \tag{26a}$$

$$\psi(0,y) = 0 \tag{26b}$$

$$\forall z,\ y \geq \delta(z) \qquad C_i(z,y) = C_{i,r} \tag{26c}$$

$$\psi(z,y) = 0 \tag{26d}$$

It is worth mentioning that layer thickness is not required for simulation. The concentration profiles are calculated in viscous and buffer sublayers all along the membrane, independently of layer thickness. Thickness value could nevertheless be estimated a posteriori from concentration profiles. This point is a major advantage of the PPTM compared with film model or other 1-D models, especially in the case of ionic mixtures for which theory leads to a layer thickness for each ion.

This system of equations is solved by the Gaussian elimination method. This proceeding is iterated all along the membrane ($z = 0$ to L corresponding to $k = 1$ to m steps) and average permeate concentrations $\overline{C_{i,p}}$ and permeation flux $\overline{J_v}$ are calculated by Eqs. 27 and 28. This procedure is performeed until $\overline{C_{i,p}}$ converges on a constant value.

$$\overline{C_{i,p}} = \frac{\sum_{k=1}^{m} J_v(z_k) C_{i,p}(z_k)}{\sum_{k=1}^{m} J_v(z_k)} \tag{27}$$

$$\overline{J_v} = \frac{\sum_{k=1}^{m} J_v(z_k)}{m} \tag{28}$$

In this model, it was considered that each j-step is independent which means that no radial mixing occurs at the active layer outlet and that mixing appears only in the support layer or in the permeate compartment. It should be noted that other visions presented in a previous article[20] gives the same average values even if profiles along the membrane are slightly different.

Table 2. Membrane Characteristics

Membrane Characteristics	Data	Data Assessment
Material	Polyamide	Supplier
Length (m)	1.20	Supplier
Internal diameter (mm)	12.7	Supplier
Area (10^{-4} m^2)	1.27	Supplier
Hydraulic permeability (10^{-14} m^3 m$-^2$)	1.6	Water flux measurements
Mean pore radius (nm)	0.53	Glucose rejection + model

Experimental part

The filtration set-up consists of a tubular AFC 40 membrane from PCI Membrane Systems Ltd fed by a volumetric pump at given pressure and flow rate. The membrane characteristics are summed-up in Table 2. Concentrations are kept constant by recycling both permeate and retentate streams into the feed tank. Solutions were cooled in a counter-current heat exchanger to regulate the temperature at 25°C.

Permeate stream was weighted and analyzed by ionic chromatography (ICS 1000, Dionex, Voisins le Bretonneux, France) equipped with a conductivity detector. Experiments were carried out for an applied pressure in the range between 5 and 25 bars and for a feed stream varying from 700 to 1800 L h^{-1}.

Six ionic solutions (i.e., 3 pure salt solutions, 2 ternary, and 1 quaternary mixtures) are made by dissolving various salt quantities in demineralized water with a residual conductivity lower than 0.1 μS cm^{-1}.

Membrane permeability L_p was estimated before each experiment from a water flux to check that membrane hydrodynamic properties were modified during the campaign of experiments. The set-up was running during one night at $Q = 1$ m^3 h^{-1} and $\Delta P = 10$ bar before each experiments to reach ionic adsorption equilibrium.

Mean pore radius was assessed by adjusting its value in the model to correctly describe the real rejection of glucose for which only steric effects act on rejection as it is usually done in literature (Bowen et al.,[22] Escoda et al.[43]) and precisely described in a previous article.[20]

For each experiment, observed rejections $R_{i,obs}$ were calculated from concentrations of both permeate and retentate streams at various applied pressures ΔP and tangential velocities U_t.

The values of ε_p and X_d were identified by fitting, with the 1-D membrane transport model, the real rejections $R_{i,m}$. For single salt mixtures, ε_p was assessed for concentrated solutions by neglecting charge influence and X_d was then identified with the diluted solution studied. For ternary and quaternary mixtures, both ε_p and X_d were identified simultaneously by adjusting their value to describe the three or four rejection curves. Indeed, with ionic mixtures, only one couple (ε_p, X_d) can describe the selectivity between the various ions.[44]

Real rejections were previously calculated from observed rejection curves at various U_t with the VVM.[14,45] This method consists in extrapolating observed rejections at infinite velocities for which polarization phenomenon no more exists and wall concentrations $C_{i,w}$ are equal to retentate ones $C_{i,r}$ ($R_{i,m} = \lim_{U_t \to \infty} R_{i,obs}$). $R_{i,m}$ and $R_{i,obs}$ are thus linked by means of a mass transfer coefficient k between the bulk solution and the membrane wall, through the film law:

$$\ln\left(\frac{1-R_{i,\mathrm{obs}}}{R_{i,\mathrm{obs}}}\right)=\ln\left(\frac{1-R_{i,\mathrm{m}}}{R_{i,\mathrm{m}}}\right)+\frac{J_\mathrm{v}}{k} \tag{29}$$

The value of k could be estimated by means of a empirical Sherwood correlation[46] (Deissler equation in our case) and experimental evolution of rejection with velocity.[20] This method was used to estimate the parameters describing the transfer through the membrane (i.e., r_p, ε_p, and X_d) and to check if the PPTM correctly describe the membrane transport.

Results and Discussion

In this article, experimental and simulated (with the PPTM) separation performances are presented for various experimental conditions. The aim of this part is to check if the PPTM allows a well description of the polarization layer experiment in the presence of several ions. In practice, this validation is investigated by studying the evolution of rejection curves with the tangential velocity for various single salt solutions and mixtures.

The values of the various parameters of the membrane transport model, i.e., the membrane permeability L_p, the mean pore radius r_p, the dielectric constant within the pores ε_p, and the membrane charge density X_d, are those presented in previous articles (for pure salt solutions[20,40] and for ternary ionic mixtures[44]). The values of L_p and r_p are constant whatever the solution filtrated and obtained values are $L_\mathrm{p} = 1.6 \times 10^{-14}$ m^3 m^{-2} and $r_\mathrm{p} = 0.53$ nm.

The values of ε_p and X_d were estimated by fitting the real rejection curves (calculated by the VVM) with the 1-D transport model within the membrane (DSPM). In the case of single salt solutions, it exists an infinity of couples (ε_p, X_d) describing one salt rejection curve and the couple (ε_p, X_d) is thus obtained by fitting successively a concentrated and the diluted salt solutions. In the case of mixtures (ternary or quaternary), the parameters X_d and ε_p are estimated simultaneously from real rejection curves obtained for each ion in solution. Indeed, for each mixture filtration, there is one rejection curve per ion and the resolution is thus constrained or overconstrained, i.e., two or more independent curves described by only two adjustable parameters. The values of ε_p and X_d and their evolutions with experimental conditions are not discussed in the article, but they are summed up in Table 3. Nevertheless, it should be noticed that the obtained values are coherent with other studies. Indeed, some authors (Senapati and Chandra,[47] Wang and Anderko[48]) have found dielectric constant ε_p close to 50–60 for pure salt solutions. Moreover, the ε_p-values identified from mixtures are also consistent with the values assessed with pure salt solutions. Indeed, ε_p was found to decrease within the pore and more the solution contains divalent more its value is small (linear trend was found with proportion of divalent). The values of the membrane charge X_d are also in the same range that those presented by other authors (Mazzoni and Bandini[49]). X_d-values are found to strongly depend with the salt filtrated due to the different adsorption of the various ions on the membrane material (Bandini et al.[50]). Adequacy was also found between the values identified with pure salt solutions and mixtures (i.e., a monotonous behavior of X_d-value with divalent proportion).

Table 3. Values of the Parameters ε_p and X_d Leading to the Best Simulated Description of the Various Filtration Experiments

Filtrated Solutions	Concentrations (mol m^{-3})	ε_p	X_d (mol m^{-3})	Reference
Pure NaCl	50	57.3	−65	40
Pure $MgCl_2$	25	62.2	−1.5	20
Pure Na_2SO_4	25	32	∼0	20
$NaCl/MgCl_2$ (M1)	25/12.5	51.1	−5.3	44
$NaCl/Na_2SO_4$ (M2)	25/12.5	35.7	−0.1	44
$MgCl_2/Na_2SO_4$ (M3)	5.5/5.5	56.9	−5.7	–

These various couples (ε_p, X_d) estimated from real rejection with the DSPM are introduced in the PPTM to describe observed rejection curves.

The α-parameter representing the diffusivity increase at the membrane wall, which governs the polarization layer establishment, is discussed to check the influence of an electrical potential in the layer. For each simulation, the α-coefficient describing the diffusivity increase at the membrane wall is calculated from the tangential velocity by Eq. 25. In this article, simulations are compared with experimental observed and real rejections obtained for the various studied solutions.

Validation on pure salt solutions

Experimental and simulated rejection curves obtained for pure salt solutions (NaCl and $MgCl_2$) are drawn on Figures 2a, b. The experimental real rejections are estimated by the VVM, and the experimental observed rejection are measured for three various tangential velocities.

From these figures, it can be concluded that the α-parameter estimated with the first version of the PPTM (without electrical potential in the flow) is suitable to describe the transport of pure salts in the polarization layer, and especially the influence of pressure and tangential velocity on rejection. These observations indicate that considered a diffusivity increase at the membrane wall is required to correctly describe the polarization layer establishment even if the variation of activity coefficients is taken into account. Indeed, in the case of pure salt solutions, introduction of an electric gradient in the layer was found to have no effect on the α value as it is equivalent to the way in which a mean diffusivity is considered. It is worth mentioning that rejection of Na_2SO_4 is also well described by the PPTM but results are not presented here because of the small rejection variations with velocity.

Figure 3 shows an example of the evolution of the concentration profile along the membrane for a 50 mol m^{-3} NaCl solution. This figure reveals that concentration increases up to 15% between bulk and membrane wall at this pressure (15 bar) but it can even increases up to 25% for higher applied pressures (e.g., 25 bar). It should also be noted that heterogeneity along the membrane is significant and should not be neglected, especially with short membranes for which edge effects are predominant. These observations clearly prove that a suitable model describing the 2-D layer establishment is required to accurately describe the selectivity of membrane separation, giving its legitimacy to this study.

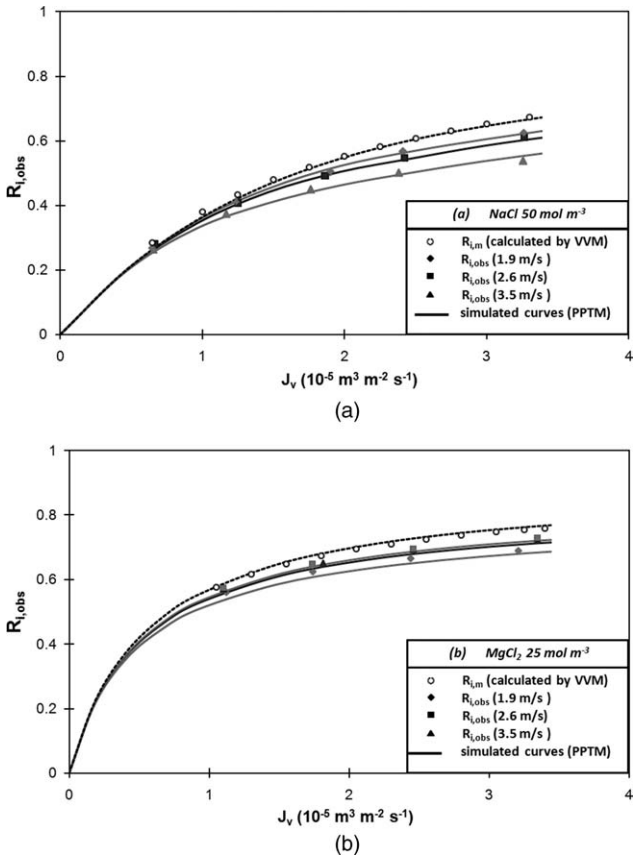

Figure 2. (a) Observed and real rejection curves obtained experimentally (symbols) and simulated (lines) for solutions of (a) NaCl 50 mol m^{-3} and (b) $MgCl_2$ 25 mol m^{-3}.

Validation on ternary mixture solutions

In the opposite of pure salt solutions, with ionic mixtures, a mean diffusivity cannot be considered as each ion diffuses at its own velocity. For this reason, an electrical gradient has to be introduced to respect electroneutrality and only the new version of the PPTM can model the 2-D multi-ionic transport through the polarization layer.

In this article, two kinds of ternary mixture are studied. The former contains a divalent cation Mg^{2+} when the latter contains a divalent anion SO_4^{2-}. Both mixtures are also made of two monovalent ions, Na^+ and Cl^-. Filtration and simulations of these two kinds of mixtures were performed for three proportions of divalent ion compared with that of noncommon monovalent ion in eq m^{-3}. In this part, only the intermediate proportion 50/50 of the two kinds of mixture is presented (i.e., M1 and M2). Parameters governing the transfer through the membrane for these two mixtures were discussed in a previous article[44] and they are summed-up in Table 3.

Simulations were performed by considering the linear law (Eq. 29) linking the α-value to the tangential velocity U_t obtained with the old version of PPTM (cf., Déon et al.[20,40]) and validated at the previous paragraph.

The experimental and simulated rejection curves of the three ions in solution are given on Figures 4a and b for three tangential velocities and for the $NaCl/MgCl_2$ (a) and $NaCl/Na_2SO_4$ (b) mixtures.

Real rejections are not depicted in these figures, but they are presented for the three proportions in a previous article.

As shown by these figures (Figure 4a and b), the PPTM seems to correctly describe rejection evolutions with the permeation flux and especially the negative rejections obtained for the no-common ion at low fluxes. But the advantage of the PPTM comes from being able to simulate the influence of cross-flow velocity on observed rejection. From curves comparison, it can be concluded that the influence of velocity on the polarization layer, and so on the observed rejection, is correctly predicted by the PPTM whatever the kind of mixture studied. Even if rejection was found to increase with tangential velocity for each ion, it is worth mentioning that the facilitated transport of the noncommon monovalent ion at low flux (i.e., showing a negative rejection) leads to the opposite behavior. Indeed for ion showing facilitated transfer through the membrane, the polarization phenomenon tends to decrease the concentration at the membrane wall. Velocity increase thus induces a higher membrane wall and so a lower rejection. This behavior is depicted on Figure 5a which shows the influence of velocity on the concentration profiles of cations in the M1 mixture (i.e., Na^+ and Mg^{2+}) under 5 bars. Unfortunately, the rejection decrease with velocity is too weak to observe it on rejection curves (cf., Figure 4a). Finally, it should be noted that rejection curves obtained for the two other proportions (i.e., 10/90 and 90/10) are not presented in this article, but the quantitative influence of velocity on rejection is well predicted irrespective of the nature of the filtrated solution. This observation confirms that the α-parameter representing the diffusivity increase at

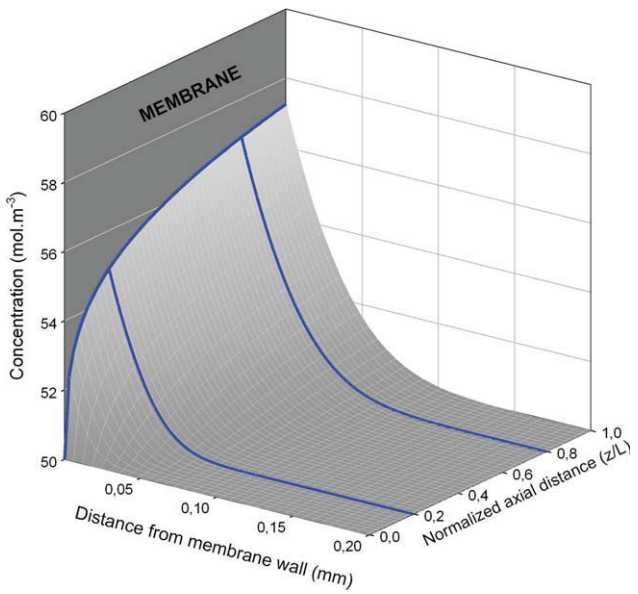

Figure 3. Simulated concentration polarization layer establishment along the membrane for a 50 mol m^{-3} NaCl solution (with U_t = 2.6 m s^{-1} and ΔP = 15 bar).

[Color figure can be viewed in the online issue, which is available at wileyonlinelibrary.com].

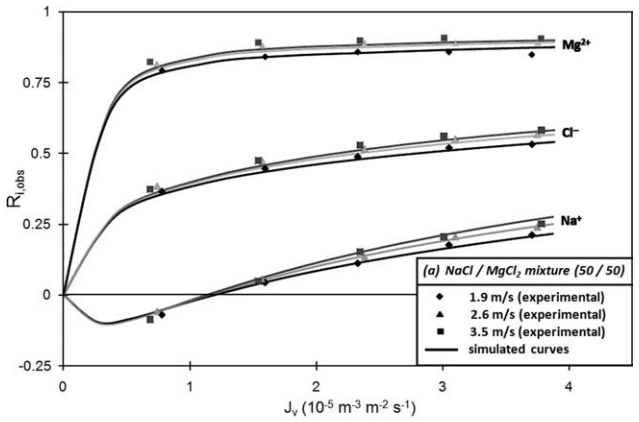

(a)

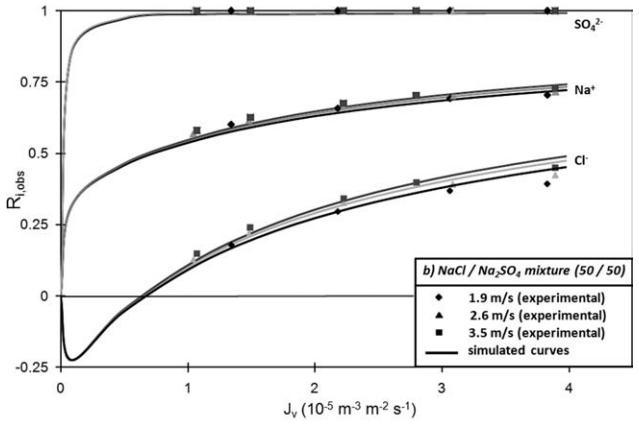

(b)

Figure 4. Observed rejection curves obtained for three tangential velocities (◆ = 1.9 m s^{-1}, ▲ = 2.6 m s^{-1}, ■ = 3.5 m s^{-1}) with (a) NaCl/$MgCl_2$ and (b) NaCl/Na_2SO_4 mixtures.

the membrane wall properly modelled the polarization layer evolution with experimental conditions even for ternary mixtures.

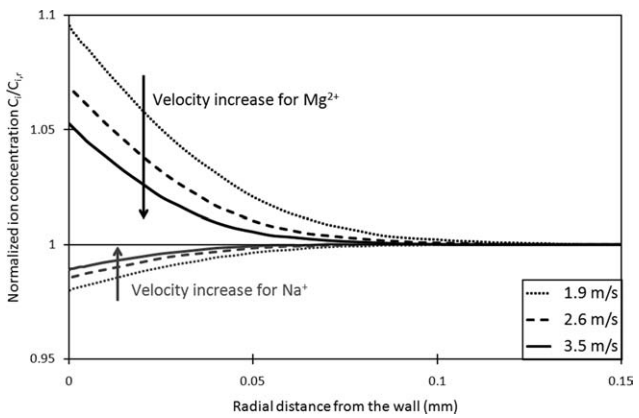

Figure 5. Normalized concentration profiles of Na^+ and Mg^{2+} for three tangential velocities at the middle of the membrane obtained with the M1 mixture (ΔP = 5 bar).

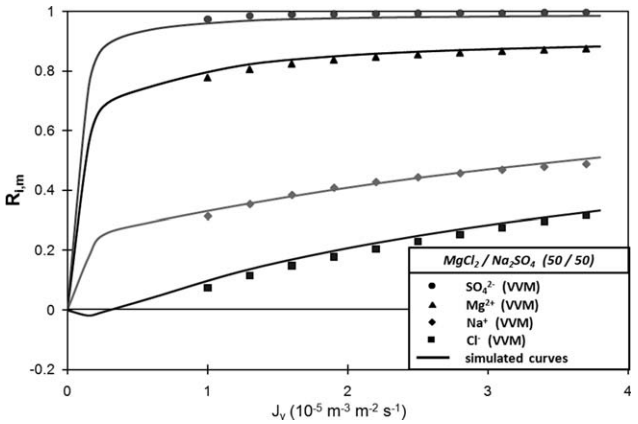

Figure 6. Real rejection curves obtained experimentally (symbols) and simulated (lines) for a Na_2SO_4/$MgCl_2$ quaternary mixtures.

Validation on a quaternary mixture solution

The same simulations were performed with a quaternary solution (M3) containing Mg^{2+}, SO_4^{2-}, Na^+, and Cl^-. The values of ε_p and X_d are simultaneously identified to fit the four curves and it was found that $\varepsilon_p = 56.9$ and $X_d = -5.7$ mol m^{-3} is the best couple of parameters to describe the selectivity between these ions. The agreement between experimental rejection and those simulated with these adjusted values is shown on Figure 6. This agreement proves that the transport within the membrane is well described by the model even when the resolution is overconstrained, i.e., four curves fitted (three independent curves and the last linked to the others by electroneutrality) with only two parameters. This conclusion suggests that filtration of complex solutions containing more than four ions could probably be described by the model and the methodology could thus be suitable for industrial applications such as partial desalination of seawater or wastewater treatment.

Concentration polarization induced by the filtration of this quaternary solution is investigated through the study of observed rejections. Figure 7 depicts the experimental and

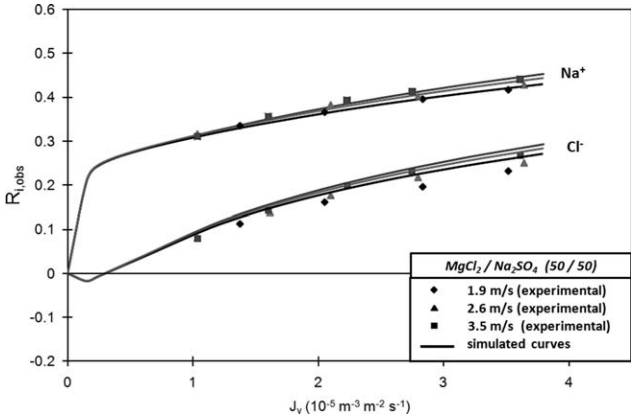

Figure 7. Observed rejection curves of Na^+ and Cl^- obtained for three tangential velocities (◆ = 1.9 m s^{-1}, ▲ = 2.6 m s^{-1}, ■ = 3.5 m s^{-1}) with a $MgCl_2$/Na_2SO_4 quaternary solution.

simulated evolution of observed rejection curves with tangential velocity for this quaternary mixture. But, for need of clarity, only rejections of monovalent ions are drawn on this graph. Experimental and simulated curves of divalent ions are also in good agreement but because of the weak sensibility on rejection, their study is not relevant.

Comparison between experimental values and simulated curves indicates that the polarization phenomenon occurring for quaternary solutions is also well described by the PPTM. As shown on this figure, very good agreement is found for rejection of Na^+. In the case of Cl^-, rejection appears to be somewhat overestimated by the model. This slight overestimation can be probably attributed to the fact that the concentrations increase at the membrane wall would tend to a slight modification of the membrane charge. Indeed, in the case of mixtures, laws linking X_d to concentrations are not available for the time being. For this reason, the PPTM cannot take account of polarization influence on the X_d-value which is probably weakly different from that estimated with the DSPM. The X_d-value can thus be probably weakly overestimated which could explain small overestimation for Cl^- as it is very sensitive to the X_d-value. However, the lack of data for quaternary mixture does not allow the charge adjustment. Introducing a law of competitive adsorption in the model appears thus to be a major way of improvement for the prediction of mixtures separations.

Nevertheless, it should be noted that the polarization influence is correctly predict as gaps between curves is agreeing and so polarization establishment appears to be well predicted whatever the solution filtrated.

Conclusion

Although the transport of ions through the membrane seems to be often studied in the literature, little attention has been paid so far to the contribution of the concentration polarization on separation performances. Indeed, polarization is usually neglected or indirectly assessed. Even if some authors have developed 2-D models, results are often not compared with experimental data. On the contrary, this study is particularly focused on the polarization layer establishment during filtration of ionic solutions. The previous version of the PPTM was established and validated only for pure salt solutions. In this article, the PPTM is improved to predict the separation of multi-ionic mixtures by including an electrical gradient in the polarization layer. Comparison between experimental and simulated results has clearly shown that the influence of various experimental conditions (i.e., applied pressure, feed flow-rate or mixture proportions) is accurately described by the model. This study shows that the PPTM has the potential to become a valuable tool for industrial processes.

Full prediction of experimental selectivity between ions in complex mixture is probably quite ambitious at the present time but the findings of this study reveal that it can surely be described by a knowledge model.

Acknowledgments

The authors thank the French Ministry of Research and technology for their financial support.

Notation

a_i = activity of ion i (mol m^{-3})
A_k = membrane porosity (dimensionless)
c_i = concentration of ion i within the pore (mol m^{-3})
C_i = concentration of ion i within the polarization layer (mol m^{-3})
$C_{i,p}$ = permeate concentration of ion i (mol m^{-3})
$C_{i,r}$ = bulk concentration of ion i (mol m^{-3})
$C_{i,w}$ = wall concentration of ion i (mol m^{-3})
$D_{i,\infty}$ = molecular diffusion coefficient of ion i at infinite dilution (m^2 s^{-1})
$D_{i,m}$ = molecular diffusion coefficient of ion i (m^2 s^{-1})
$D_{i,p}$ = pore diffusion coefficient of ion i (m^2 s^{-1})
$D_{i,t}$ = turbulent diffusion coefficient of ion i (m^2 s^{-1})
$D_{i,w}$ = diffusion coefficient of ion i at the wall (m^2 s^{-1})
E = electronic charge (1.602177×10^{-19} C)
F = Faraday constant (96487 C mol^{-1})
I = ionic strength (mol m^{-3})
j_i = ionic flux of ion i (mol (m^{-2} s^{-1}))
J_v = volumetric permeation flux (m^3 (m^{-2} s^{-1}))
k = mass transfer coefficient (m s^{-1})
k_B = Boltzmann constant (1.38066×10^{-23} J K^{-1})
$K_{i,c}$ = ionic hindrance factor for convection (dimensionless)
$K_{i,d}$ = ionic hindrance factor for diffusion (dimensionless)
L = membrane length (m)
L_p = water permeability (m^3 m^{-2})
m = number of steps along the membrane length
R = universal gas constant (8.314 J (mol^{-1} K^{-1}))
r_i = Stokes radius of ion i (m)
$R_{i,m}$ = real rejection of ion i (dimensionless)
$R_{i,obs}$ = observed rejection of ion i (dimensionless)
r_p = average pore radius (m)
T = temperature (K)
U = axial velocity within the flow (m s^{-1})
U_t = average tangential velocity (m s^{-1})
v = radial velocity within the flow (m s^{-1})
$\vec{V}$ = velocity vector in the flow (m s^{-1})
x = axial position within the pore (m)
X_d = membrane effective charge density (mol m^{-3})
y = radial wall distance (m)
z = axial position along the membrane (m)
z_i = valence of ion i (dimensionless)

Greek letters

α = factor manifesting diffusion increase at the wall (dimensionless)
ΔP = applied pressure (Pa)
ΔW_i = solvation energy barrier (J)
Δx = membrane thickness (m)
$\Delta\psi_D$ = Donnan potential (V)
$\Delta\pi$ = osmotic pressure difference (Pa)
ϕ_i = steric partition coefficient (dimensionless)
ϕ'_i = partition coefficient including activity coefficient, steric, and dielectric effects
ψ = electrical potential within the pore (V)
δ = polarization layer thickness (m)
ε_0 = permittivity of free space (8.85419×10^{-19} C)
ε_b = bulk dielectric constant (dimensionless)
ε_p = pore dielectric constant (dimensionless)
$\gamma_{i,m}$ = activity coefficient of ion i in the pore side of the interface (dimensionless)
$\gamma_{i,s}$ = activity coefficient of ion i in the solution side of the interface (dimensionless)
η = dynamic viscosity within pores (Pa s)
λ_i = ratio of ion stokes radius to pore radius (dimensionless)

Literature Cited

1. Van der Bruggen B, Everaert K, Wilms D, Vandecasteele C. Application of nanofiltration for removal of pesticides, nitrate and hardness from ground water: rejection properties and economic evaluation. *J Membr Sci*. 2001;193:239–248.
2. Van der Bruggen B, Schaep J, Maes W, Wilms D, Vandecasteele C. Nanofiltration as a treatment method for the removal of pesticides from ground waters. *Desalination*. 1998;117:139–147.

3. Pontié M, Diawara C, Lhassani A, Dach H, Rumeau M, Buisson H, Schrotter JC. Chapter 2 Water Defluoridation Processes: A Review. Application: Nanofiltration (NF) for Future Large-Scale Pilot Plants. In: *Advances in Fluorine Science*. 2006;2:49–80.
4. Oumar Anne C, Trebouet D, Jaouen P, Quemeneur F. Nanofiltration of seawater: fractionation of mono- and multi-valent cations. *Desalination*. 2001;140:67–77.
5. Pontié M, Lhassani A, Diawara CK, Elana A, Innocent C, Aureau D, Rumeau M, Croue JP, Buisson H, Hemery P. Seawater nanofiltration for the elaboration of usable salty waters. *Desalination*. 2004;167:347–355.
6. Walha K, Amar RB, Bourseau P, Jaouen P. Nanofiltration of concentrated and salted tuna cooking juices. *Process Saf Environ Protect*. 2009;87:331–335.
7. Bourseau P, Vandanjon L, Jaouen P, Chaplain-Derouiniot M, Massé A, Guérard F, Chabeaud A, Fouchereau-Péron M, Le Gal Y, Ravallec-Plé R, Bergé JP, Picot L, Piot JM, Batista I, Thorkelsson G, Delannoy C, Jakobsen G, Johansson I. Fractionation of fish protein hydrolysates by ultrafiltration and nanofiltration: impact on peptidic populations. *Desalination*. 2009;244:303–320.
8. Pontié M, Dach H, Leparc J, Hafsi M, Lhassani A. Novel approach combining physico-chemical characterizations and mass transfer modelling of nanofiltration and low pressure reverse osmosis membranes for brackish water desalination intensification. *Desalination*. 2008;221:174–191.
9. Hagmeyer G, Gimbel R. Modelling the salt rejection of nanofiltration membranes for ternary ion mixtures and for single salts at different pH values. *Desalination*. 1998;117:247–256.
10. Tanninen J, Manttari M, Nystrom M. Effect of salt mixture concentration on fractionation with NF membranes. *J Membr Sci*. 2006; 283:57–64.
11. Gekas V, Olund K. Mass transfer in the membrane concentration polarization layer under turbulent cross flow: II. Application to the characterization of ultrafiltration membranes. *J Membr Sci*. 1988;37: 145–163.
12. Afonso MD, De Pinho MN. Mass transfer modeling for salt transport in amphoteric nanofiltration membranes. *Ind Eng Chem Res*. 1998;37:4118–4127.
13. Cavaco Morão AI, Brites Alves AM, Geraldes V. Concentration polarization in a reverse osmosis/nanofiltration plate-and-frame membrane module. *J Membr Sci*. 2008;325:580–591.
14. Jonsson G, Boesen CE. Concentration polarization in a reverse osmosis test cell. *Desalination*. 1977;21:1–10.
15. Geraldes V, Afonso MD. Prediction of the concentration polarization in the nanofiltration/reverse osmosis of dilute multi-ionic solutions. *J Membr Sci*. 2007;300:20–27.
16. Cavaco Morão AI, Szymczyk A, Fievet P, Brites Alves AM. Modelling the separation by nanofiltration of a multi-ionic solution relevant to an industrial process. *J Membr Sci*. 2008;322:320–330.
17. Bhattacharjee S, Chen JC, Elimelech M. Coupled model of concentration polarization and pore transport in cross flow nanofiltration. *AIChE J*. 2001;47:2733–2745.
18. Pak A, Mohammadi T, Hosseinalipour SM, Allahdini V. CFD modeling of porous membranes. *Desalination*. 2008;222:482–488.
19. Verliefde ARD, Cornelissen ER, Heijman SGJ, Verberk JQJC, Amy GL, Van der Bruggen B, van Dijk JC. Construction and validation of a full-scale model for rejection of organic micropollutants by NF membranes. *J Membr Sci*. 2009;339:10–20.
20. Déon S, Dutournié P, Bourseau P. Modeling nanofiltration with Nernst-Planck approach and polarization layer. *AIChE J*. 2007;53:1952–1969.
21. Bowen WR, Mukhtar H. Characterisation and prediction of separation performance of nanofiltration membranes. *J Membr Sci*. 1996; 112:263–274.
22. Bowen WR, Mohammad AW, Hilal N. Characterisation of nanofiltration membranes for predictive purposes—use of salts, uncharged solutes and atomic force microscopy. *J Membr Sci*. 1997;126:91–105.
23. Donnan FG. Theory of membrane equilibria and membrane potentials in the presence of non-dialysing electrolytes. A contribution to physical-chemical physiology. *J Membr Sci*. 1995;100:45–55.
24. Ferry JD. Statistical evaluation of sieve constants in ultrafiltration. *J Gen Physiol*. 1935;20:95–104.
25. Van der Bruggen B, Vandecasteel C. Modelling the retention of uncharged molecules with nanofiltration. *Water Res*. 2002;36:1360.
26. Aimar P, Meireles M, Sanchez V. A contribution to the translation of retention curves into pore size distributions for sieving membranes. *J Membr Sci*. 1990;54:321–338.
27. Born M. Volumen and hydratationswärme der ionen. *Z Physik Chem*. 1920;1:45.
28. Yaroshchuk AE. Dielectric exclusion of ions from membranes. *Ad Colloid Interf Sci*. 2000;85:193–230.
29. Yaroshchuk AE. Non-steric mechanisms of nanofiltration: superposition of Donnan and dielectric exclusion. *Sep Purif Technol*. 2001; 22–23:143–158.
30. Schlögl R. Membrane permeation in system far from equilibrium. Berichte der Bunsengesellschaft Physik Chem. 1966;70:400.
31. Dresner L. Some remarks on the integration of extended Nernst-Planck equation in the hyperfiltration of multicomponent solutions. *Desalination*. 1972;10:27–46.
32. Deen WM. Hindered transport of large molecules in liquid-filled pores. *AIChE J*. 1987;33:1409–1425.
33. Anderson JL, Quinn JA. Restricted transport in small pores: a model for steric exclusion and hindered particle motion. *Biophys J*. 1974; 14:130–150.
34. Bowen WR, Welfoot JS. Modelling the performance of membrane nanofiltration-critical assessment and model development. *Chem Eng Sci*. 2002;57:1121–1137.
35. Bhattacharya S, Hwang S-T. Concentration polarization, separation factor, and Peclet number in membrane processes. *J Membr Sci*. 1997;132:73–90.
36. Van den Berg GB, Racz IG, Smolders CA. Mass transfer coefficients in cross-flow ultrafiltration. *J Membr Sci*. 1989;47:25–51.
37. Bhattacharjee S, Kim AS, Elimelech M. Concentration polarization of interacting solute particles in cross-flow membrane filtration. *J Colloid Interf Sci*. 1999;212:81–99.
38. Padet J. *Fluides en écoulements*. Paris: Masson; 1990.
39. Bird RB, Stewart WE, Lightfoot EN. *Transport phenomena*. New York: Wiley; 2002.
40. Déon S, Dutournié P, Bourseau P. Transfer of monovalent salts through nanofiltration membranes: a model combining transport through pores and the polarization layer. *Ind Eng Chem Res*. 2007;46:6752–6761.
41. Eickstein EC, Bailey DG, Shapiro AH. Self-diffusion of particles in shear flow of a suspension. *J Fluid Mech*. 1977;79:191–208.
42. Picioreanu C, Van Loosdrecht MCM, Heijnen JJ. A theoretical study on the effect of surface roughness on mass transport and transformation in biofilms. *Biotechnol Bioeng*. 2000;68:355–369.
43. Escoda A, Fievet P, Lakard S, Szymczyk A, Déon S. Influence of salts on the rejection of polyethyleneglycol by an NF organic membrane: pore swelling and salting-out effects. *J Membr Sci*. 2010;347: 174–182.
44. Déon S, Dutournié P, Limousy L, Bourseau P. Transport of salt mixtures through nanofiltration membranes: numerical identification of electric and dielectric contributions. *Sep Purif Technol*. 2009;69:225–233.
45. Nakao S, Kimura S. Analysis of solutes rejection in ultrafiltration. *J Chem Eng Jpn*. 1981;14:32–37.
46. Gekas V, Hallstrom B. Mass transfer in the membrane concentration polarization layer under turbulent cross flow: I. Critical literature review and adaptation of existing Sherwood correlations to membrane operations. *J Membr Sci*. 1987;30:153–170.
47. Senapati S, Chandra A. Dielectric constant of water confined in a nanocavity. *J Phys Chem B*. 2001;105:5106–5109.
48. Wang P, Anderko A. Computation of dielectric constants of solvent mixtures and electrolyte solutions. *Fluid Phase Equilibria*. 2001; 186:103–122.
49. Mazzoni C, Bandini S. On nanofiltration Desal-5 DK performances with calcium chloride-water solutions. *Sep Purif Technol*. 2006;52: 232–240.
50. Bandini S. Modelling the mechanism of charge formation in NF membranes: theory and application. *J Membr Sci*. 2005;264:75–86.

Manuscript received Feb. 11, 2010, and revision received May 6, 2010.